Combustion and Flame 234 (2021) 111644

Contents lists available at ScienceDirect

Combustion and Flame

journal homepage: www.elsevier.com/locate/combustflame

Flame spread predictions over linear discrete fuel arrays using an empirical *B*-number model and stagnation point flow

Giovanni Di Cristina[a], Nicholas S. Skowronski[b], Albert Simeoni[c], Ali S. Rangwala[c,*], Seong-kyun Im[a,d,*]

[a] Department of Aerospace and Mechanical Engineering, University of Notre Dame, Notre Dame, IN, United States
[b] USDA Forest Service, Northern Research Station, Morgantown, WV, United States
[c] Department of Fire Protection Engineering, Worcester Polytechnic Institute, 50 Prescott St., Worcester, MA 01605, United States
[d] Department of Mechanical Engineering, Korea University, 319 Innovation Hall, 145 Anam-ro Seongbuk-gu, Seoul 02841, Republic of Korea

ARTICLE INFO

Article history:
Received 5 April 2021
Revised 26 July 2021
Accepted 26 July 2021

Keywords:
B-number
Discrete fuel
Forced convection
Flame spread

ABSTRACT

A stagnation-point flow model based in part on the mass transfer *B*-number was adapted to approximate the heat flux and time to ignition of dowel arrays subject to forced convection flame spread. Previous work on forced flow flame spread along a dowel array has characterized the existence of discretized flame behavior. In deployment-scale wildland fire models, small fuels are smaller than the grid resolution. Sub-grid modeling then relies on empirical relationships, such as Nusselt number–Reynolds number (*Nu-Re*) models, to estimate the fire spread. Current *Nu-Re* models utilized to calculate the heat flux and ignition times predict higher heat transfer and faster ignition times with increasing flow speeds. However, analysis of the flame spread revealed that the ignition time has a parabolic relationship with the flow speed, with the fastest ignition time occurring around the onset of the discrete flame behavior. *Nu-Re* models cannot capture the upward inflection of ignition times beyond the onset of the discrete flame spread, where the ignition times increase with greater flow speeds. A boundary layer solution to the plume heat flux impinging on the next unignited dowel was employed to develop a *B*-number empirical model. The *B*-number model captures the changes to mass and heat transfer induced by differences in the flow speed and array spacing. The proposed empirical *B*-number model together with heat flux approximation generates more accurate predictions for ignition times than the existing approach.
© 2021 The Combustion Institute. Published by Elsevier Inc. All rights reserved.

1. Introduction

In recent years, wildland fires have increased in frequency and number of acres burned, leading to an average loss of 7.5 million acres of vegetation annually [1]. Although wildland fires are a natural phenomenon in many ecosystems, preventing or reducing the damage to local communities can be achieved by developing a better understanding of the processes governing the spread of wildland fires [2–4]. Wildland fires have often been described as the consecutive ignition of discrete fuel elements [5]. Accordingly, researchers have utilized discrete fuel arrays as vegetation surrogates to study wildland fire spread; these arrays have also been used in other studies examining façade, warehouse, and commodity fires [6,7]. In these scenarios, the spread of the flame depends on the spatial distribution of the fuel elements, thus simple arrays can be employed to quickly and easily modulate the spacing, arrangement, and size of the fuels. In simple arrangements, the fuels are arranged vertically [6–9] or horizontally [10] with no forced flow. In horizontal fuel arrays, the flame spread has been found to be linear with respect to time. Vogel and Williams [10] determined the time to ignition based on geometric considerations of the flame front impinging on the next unignited dowel and the heat conduction equation for thermally thick fuels. In contrast, these assumptions do not hold true for vertically arranged arrays, where the flames impinge on the next fuel element, and natural convection plays a larger role in the flame behavior, complicating the heat transfer mechanisms. Experiments on horizontal arrays and the effects of an imposed, co-current, flow have revealed an increase in the flame spread rate with increasing co-current flow speeds [11,12]. Prahl and Tien extended the work by Vogel and Williams in developing an empirical model that predicted the flame spread rate for convective flows of up to 0.9 m/s [11]. Wind was considered a pushing mechanism that tilts the flame towards unignited fuel elements, but no additional effects such as increased mixing or mass transfer were considered.

* Corresponding authors.
E-mail addresses: rangwala@wpi.edu (A.S. Rangwala), sim3@korea.ac.kr (S.-k. Im).

https://doi.org/10.1016/j.combustflame.2021.111644
0010-2180/© 2021 The Combustion Institute. Published by Elsevier Inc. All rights reserved.

Nomenclature

a	Stretch rate
B	Spalding mass transfer number
c_s	Specific heat of wood
c_p	Specific heat of air
D	Diffusion coefficient
d	Diameter
f	Normalized velocity profile
ΔH_R	Heat of reaction
h	Heat transfer coefficient
Pr	Prandtl number
Q_g	Heat of gasification
Q_c	Heat of combustion
$\dot{q}''$	Heat flux
Re	Reynolds number
s	Spacing
k_s	Thermal conductivity of wood
T	Temperature
r	Stoich. parameter
Nu	Nusselt number
t_i	Ignition time
t_{ind}	Induction time
u	Freestream velocity
x	Coordinate
$Y_{O2,\infty}$	Mass fraction of Oxygen
y	Coordinate

Greek letters

α	Flame angle
δ	Boundary layer thickness
ρ	Density
ν_∞	Kinematic air viscosity
ν_{st}	Stoich. O_2-fuel mass ratio
Λ	Damkholer number
φ	Coupling function
η	Normalized coordinate

Subscripts

∞	Ambient air, freestream
e	External
g	Gas phase
i	Ignition
r	Radiative
s	Solid
sp	Spacing

Other studies that utilized bulk or continuous fuel structures have highlighted the effects of a co-current wind on flame spread, finding that convection is the main heat transfer mechanism [13,14], while induced flow structures and vortices can play a major role in the forward propagation of wildland fires [15]. With solid fuel ignition, increasing flow speeds can affect ignition time scales [16]. Generally, the time to ignition of a solid is taken as the time to pyrolysis because the mixing and chemical times are significantly shorter. A freestream flow will increase the heat transfer and thus decrease the pyrolysis time. If the flow speeds are relatively low, as is the case with natural convection [8,9] or in Prahl and Tien's [11] study, the resulting ignition time is faster. However, a monotonous decrease in the ignition time with increasing flow speeds does not continue indefinitely. At a certain critical flow speed, an inflection point occurs after which increasing the flow speed further leads to increasing ignition times [16,17]. A high flow velocity leads to greater mass transfer and turbulence, reducing the mixing time. However, due to the increased convective cooling and shorter residence times, the rate of rise in the gas phase temperature and the proceeding reaction rate are slower, resulting in higher induction times and ultimately longer ignition times. The trends described are for a single cylinder in cross-flow, and it has been found that analogous behavior occurs in cylinder arrays [18,19].

Prior work performed by the authors has found that the faster flame propagation along arrays was not necessarily linked to faster wind speeds [18]. Furthermore, because of the changing time scales as the flow speed increases, the behavior of the flame itself changes. At low flow speeds, the resulting flame is continuous, with each flaming fuel element contributing to the larger flame area. As the flow speed increases, not only do the time scales shift but the vorticity and turbulence surrounding the array also increase [20]. The flame behavior shifts at faster flow speeds, creating fragmented and discretized flames. Under this discrete flame behavior regime, each fuel element burns simultaneously but feature individual (or discrete) flames anchored to the fuel element surface rather than one continuous flame area [19].

Because of the low flow speeds typically used in experiments, past studies have not observed this significant shift in flame behavior [10,11]. Furthermore, because of these relatively low flow speeds, the ignition time inflection point was not attained. Generally, the heat flux is approximated using Nusselt number (Nu)–Reynolds number (Re) correlations [8,9]. These Nu-Re correlations predict a continuously increasing heat flux with higher flow speeds, resulting in fire spread predictions that are faster than what is experimentally observed. The heat flux approximation approach needs to be revised in order to capture the full spectrum of ignition time behaviors with respect to changing flow speeds.

In this study, a boundary layer stagnation-point flow model is used to estimate the heat flux [21–23]. Stagnation-point flows have been previously used to model the ignition of single cylinders in cross-flow [16,24]. The proposed heat flux model based on stagnation flow relies on the mass transfer B-number to account for the change in the mass transfer conditions [21]. The B-number, first introduced by Spalding [23] to characterize droplet combustion, relates combustion heat release to combustion losses. By utilizing experimental results, an empirical model for the B-number of the array system is developed. Flame behavior and spreading regimes for wood cribs have been associated with the B-number [25,26], thus information on the dowel array B-number aids in the understanding of the physical processes that drive fire spread. Utilizing the proposed empirical B-number model as an input for the heat flux, the ignition time is predicted and compared to predictions based on Nu-Re correlations and to the experimental results. The model developed in this study is able to predict the experimental results and accurately captures the upward inflection of the ignition time with increasing flow speeds.

2. Experimental setup

The experiments in this study were conducted in a benchtop wind tunnel that allowed for uniform and steady flows of up to approximately 5 m/s. The wind tunnel's cross sectional flow area was 15.24 cm by 15.24 cm and a total test section length of 81.28 cm, as shown in Fig. 1. The flow field was measured with a combination of pitot probes and a hot-wire anemometer. The vertical flow profile was found to be uniform. Fluctuations in the mean flow were approximately ± 5%. The pilot ignition height was set to avoid interference from the wind tunnel boundary layer.

The dowel arrays were composed of 11 wooden pine dowels (numbered 0 to 10) and a pilot wick 1 cm in front of the first dowel position. Each dowel was 3.2 mm in diameter. The flow was initialized prior to ignition, after which 0.1 ml of Dodecane was dropped onto the pilot wick and ignited. The ignition of the dowel

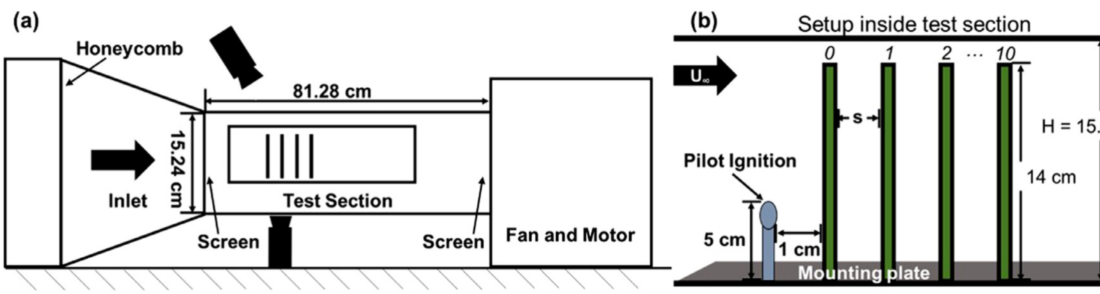

Fig. 1. Schematics of (a) the benchtop wind tunnel and (b) the dowel array setup inside the wind tunnel test section. The dowels utilized were made from pine with a diameter of 3.2 mm. The wind tunnel test section featured a square duct with 15.24 cm by 15.24 cm dimensions. (For interpretation of the references to color in this figure legend, the reader is referred to the web version of this article.)

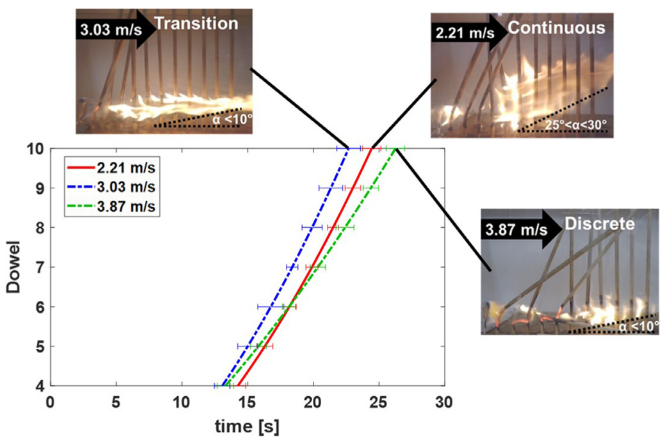

Fig. 2. Experimental flame spread data for a 1.00-cm spaced array at three flow speeds. The curves represent the quadratic fit of the average of three experiments. The three curves shown correspond to the different flame behavior regimes, both continuous (2.21 m/s) and discrete (3.87 m/s) regimes are shown, as well as a case in the transition band (3.03 m/s).

right after the pilot flame (position 0) was eliminated from the reported results in order to remove the influence of the pilot flame on the data. The flame spread was recorded from the front and top views at 60 Hz with a GoPro Hero 5 camera and a Sony DSC3, respectively. Each spacing/flow- velocity combination was repeated three times.

3. Experimental results

The flame spread behavior along the discrete dowel array depends on the flow speed and the spacing between the fuel elements. The flame behavior can be categorized into three regimes: continuous, discrete, and quenching [19]. The late-stage fire spread results (dowel positions 4 to 10) for a 1.00-cm spaced array with three flow speeds are presented in Fig. 2. The two spreading regimes, continuous and discrete, can be observed, with the 3.03 m/s flow falling within a transitional zone between the behavior regimes.

At the slowest flow speed (2.21 m/s), the flame is continuous and the speed of the flame spread is intermediate. At a fixed spacing, imposing a freestream flow initially tilts the flame towards the unignited cylinders in the array. At this stage, the flow momentum and buoyancy are comparable, and the flames form one continuous flame area, leading to a greater burning height along each dowel. As more array positions ignite, the flames merge into a larger flame area.

As the flow speed increases further, the flame tilt continues to increase until the flames flatten (i.e., their angle to the horizontal becomes very low). Thus, the upward buoyancy is overcome by the flow momentum and, at these faster flow speeds, the flames begin to exhibit discrete flame behavior. As shown in Fig. 2, at a flow speed of 3.03 m/s, the flame spread quickens, and the flame behavior falls within a transition zone between continuous and discrete regimes. At a flow speed of 3.87 m/s, the flame behavior is now fully discretized. The discrete flames are characterized by a shallower flame angle (α), a lower burning height, and a gap between the flame and the surrounding dowels. The fire spread at this speed is initially very rapid. However, at around the midpoint of the array, the flame begins to slow down, and the resulting flame spread is slower than with a flow of 2.21 m/s. Eventually, the flow speed becomes detrimental to flame spread, halting flame propagation. A flow speed of 3.87 m/s reaches this propagation limit, with flow speeds any faster than this leading to blow-off and the extinguishment of the array.

For the case of 1-cm spacing shown in Fig. 2, continuous flame behavior is observed from 1.0 to 2.5 m/s, and the onset of discretized flame behavior occurs at approximately 3.3 m/s. Between 2.5 m/s and 3.3 m/s, both continuous and discrete flame spread behavior is observed, and this is classified as a transition zone [19]. The implications of continuous and discrete propagating flame behavior on the flame spread rate itself are not straightforward. For instance, although discrete flame behavior generally features a smaller overall flame area than continuous flame spread, under certain conditions it can propagate faster. Conditions for the transition to discrete flames occur at different *Re* depending on the array spacing, with the onset of discrete flames occurring at higher *Re* for smaller array spacings. A previous study [19] showed that a Stanton number – Damkholer number relationship describes the onset of discrete flames at a Stanton number of approximately 0.028. The Stanton number incorporates the increase in convective heat transfer with flow speed but additionally balances it with the propensity of the flow to take away heat. Similarly, the Damkholer number accounts for changes in the mixing and chemical time scales for the range of flow conditions tested.

3.1. Flame spread

If the flame spread along an array is considered as a series of consecutive ignitions, then the spread can be modeled based on the time to ignition for each fuel element. The time to ignition for a solid is given by Fernandez-Pello [27] as

$$t_i = \underbrace{\frac{\pi}{4}\frac{\rho_s c k_s (T_i - T_\infty)^2}{\left(\dot{q}_e'' + \dot{q''}_r\right)^2}}_{t_{pyro}} - \underbrace{\frac{1}{4a}\ln\left(1 - \frac{\Gamma}{\Lambda_o}\right)}_{t_{ind}}. \tag{1}$$

The first grouped term is classified as the time to pyrolyze the solid (t_{pyro}), where ρ, c, and k_s are the density, specific heat, and thermal conductivity of the fuel, respectively, T_i and T_∞ are the ignition and ambient temperatures, respectively, and $\dot{q_e}''$ and $\dot{q_r}''$

are the external and radiative heat fluxes, respectively. The second term is the induction time (t_{ind}), where a is the flow velocity gradient in the radial direction (stretch rate), $\Gamma = 4c(E/RT_\infty)[(2 - \beta)/e^2(1- \beta^2)]$ and $\beta = T_\infty c_p/Y_F \Delta H_R$, and Λ_o is the Damkholer number for the combusting system. Because the induction time incorporates changes in the mixing ($1/4a$) and chemical time (Γ and Λ_o) scales arising from the changing flow field, it becomes increasingly important at faster flow speeds, as demonstrated by Niioka [16,17]. However, due to its strong dependence on the thermochemical properties and velocity gradient, measuring the induction time is difficult. Because the pyrolysis time is considered much larger than the other time scales, the ignition time is usually taken as the pyrolysis time [8,9,11,28]. For a thermally thick solid, and ignoring the radiation from the flame, the time to ignition is estimated as [28]

$$t_i = \frac{\pi}{4}\frac{\rho_s c k_s (T_i - T_\infty)^2}{(\dot{q}'')^2} \quad (2)$$

Generally, ρ, c, k_s, and the ignition temperatures are assumed to be constant; as such, the heat flux becomes the driving factor in determining the ignition time. *Nu-Re* correlations for cylinders in cross-flow [29] have been used to determine the heat flux in similar studies examining flame spread along vertically oriented arrays [8,9]. These correlations take the form of a power-law relationship between *Nu* and the freestream *Re*:

$$Nu = A(Re)^p \quad (3)$$

where *Nu* and *Re* are defined as

$$Nu = hd/k,$$
$$Re = ud/\nu \; .$$

Here, h is the heat transfer coefficient, d the dowel diameter, k the thermal conductivity of air, u the freestream flow velocity, and ν the kinematic viscosity of air. From these *Nu-Re* relationships, the heat transfer coefficient can be calculated. The time to ignition can then be estimated using Eq. (2), with a common method for representing the heat flux as follows [8–11]:

$$\dot{q}'' = h(T_g - T_i). \quad (4)$$

Due to the *Nu-Re* relationship, increasing flow speeds lead to higher heat fluxes and thus faster ignition. However, this does not fully capture the experimental results presented in Fig. 2. As the flame spread process enters the discrete behavior regime, the ignition times increase with flow speed until flame propagation becomes unsustainable.

A qualitative plot of the experimental time to ignition is presented in Fig. 3. A similar ignition time inflection point trend that was observed for a single cylinder by Niioka [16,17] is also observed for the flame spread propagation in the array. Furthermore, the critical flow velocity at which the ignition time begins to increase with flow speed aligns with the onset of discrete flame behavior. Fig. 3 also presents the expected *Nu-Re* model predictions for the same conditions, and past experiments with discrete fuels for no flow (Vogel and Williams [10]) and slow flow speeds (Prahl and Tien [11]) are shown for context. These past experiments fall within the continuous flame spread regime, where freestream flow increases flame spread. Previous research has used 1D conduction equations and geometric approximations for flame contact to predict the flame spread. In the continuous regime, prior to the onset of discrete flame spread, the *Nu-Re* model predicts the time to ignition (t_i) well. However, as *Re* increases, the predicted t_i decreases and deviates from the experimental trends once the flame transitions to discrete flame spread. Eventually, the flow effects are so strong that continued flame spread becomes unsustainable.

Thus, *Nu-Re* heat flux estimation produces reasonable results for only a portion of the *Re* conditions tested. As flow speeds increase, the heat flux calculated using the *Nu-Re* correlation continues to increase, producing an ignition time that is much faster than observed experimentally. The heat flux estimation fails to capture the higher convective effects due to the vortex shedding and other flow structures, which slow ignition. Furthermore, due to the exclusion of the induction time, changes in the chemical and mass transfer processes with increasing flow velocity are also ignored. Eventually, this deviation from the experimental results yields an impossibly low time to ignition even past the flame propagation limit of the experiments.

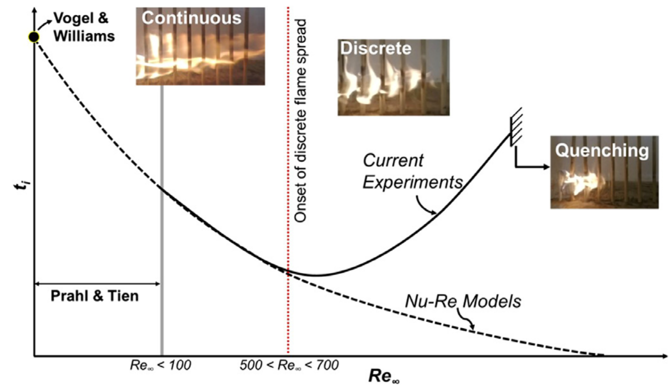

Fig. 3. Representative plot of the experimental trends compared with expected *Nu-Re* predictions. At a fixed spacing condition, the experimental data showed a decreasing ignition time as *Re* was increased up to the onset of discrete flame spread. Beyond the onset of discrete flames, the ignition times increased with higher *Re* until flame propagation ceased. A *Nu-Re* correlation, in comparison, calculates a continuously faster ignition time as *Re* increases. (For interpretation of the references to color in this figure legend, the reader is referred to the web version of this article.)

The different flame behavior regimes and a qualitative plot of the heat flux impinging on the next unignited cylinder for each scenario are depicted in Fig. 4. At a fixed spacing (s), it is observed that, as the flow speed increases, the flame behavior regimes change [19]. Furthermore, the trend in ignition time is such that the resulting heat flux is higher with increasing flow speeds up to a point (as seen in Fig. 3), after which the heat flux decreases until reaching the blow-off conditions (as evidenced by the increasing ignition times). In terms of modeling the fire spread, if the heat flux can be accurately predicted, then the flame spread from dowel to dowel can be determined. To achieve this, the changes in flow and flame behaviors must be incorporated into the heat flux estimation.

4. Modeling

4.1. Approach

The approach proposed in this study relies on a more accurate representation of the heat flux in the thermally thick time to ignition equation (Eq. (2)). To do so, the heat flux estimate developed by Annamalai and Sibulkin [21] is used. Fig. 5 presents a section of an array, showing an ignited cylinder in cross-flow upstream of an unignited cylinder. In order to predict the flame spread, the heat flux (q'') impinging on the unignited cylinder must be calculated.

The proposed model is based on the boundary layer stagnation-point flow of a single cylinder in cross-flow. When the freestream flow impacts a cylinder, a boundary layer forms on the surface where the flow must slow to satisfy the no-slip condition. A thermal boundary layer is formed for the temperature field, with the surrounding temperature field equaling the surface temperature of the solid at the solid surface. Although these two boundary layers are not necessarily the same thickness, they serve similar functions and, in this case, are represented by δ in Fig. 5. As the sur-

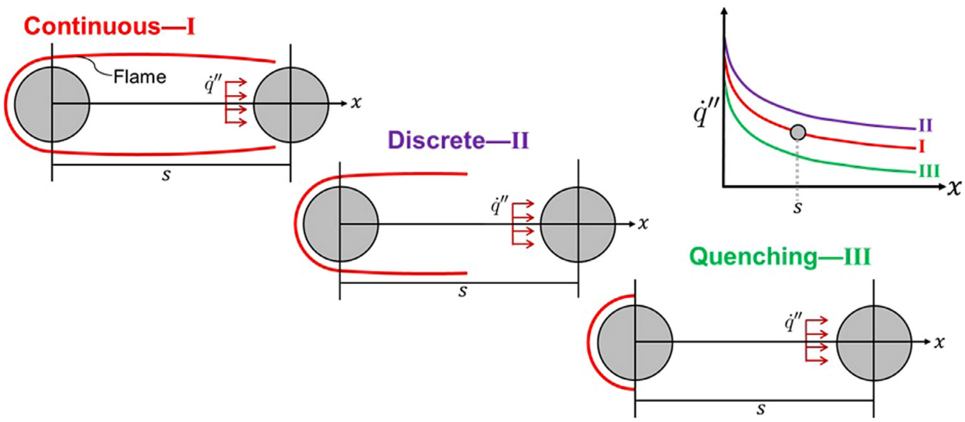

Fig. 4. Schematics of the three fire behavior regimes found in wind-driven fire spread along arrays and a qualitative plot of the heat flux over the distance between cylinders. The depicted heat flux trends are what is required in order to achieve a faster ignition time initially as the freestream flow increases, followed by a slowing down in the ignition times after the onset of discrete flame behavior. (For interpretation of the references to color in this figure legend, the reader is referred to the web version of this article.)

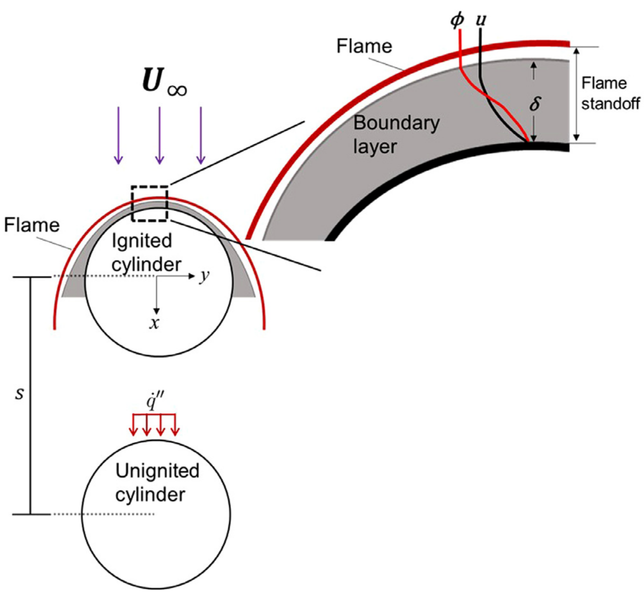

Fig. 5. Schematic of the flow over an ignited cylinder. The configuration shown was utilized by Spalding [23] and Annamalai and Sibulkin [21], an additional, unignited cylinder, which has been added downstream of the flaming cylinder to represent a subset of an array.

rounding temperature increases, in this case from the flaming upstream cylinder, an increased heat flux is delivered to the cylinder surface. The dowel surface temperature rises in response, which eventually causes the dowel cylinder to ignite. The resulting flame forms around the dowel surface and envelops the cylinder, the flame plume extending downstream and heating the next unignited cylinder [19].

The proposed model is derived from the integral energy conservation equations for a boundary layer flow at the stagnation point of a bluff body. By assuming a two-dimensional flow, the boundary layer approximation, no-slip conditions, an incompressible flow, Fickian diffusion, $Le = 1$, a non-charring fuel, no viscous dissipation, a thin flame model, and using the Schwab-Zeldovich formulation, the normalized energy–species coupling equation is defined as [21,30]

$$u\frac{\partial \phi}{\partial x} + v\frac{\partial \phi}{\partial y} = \frac{\partial}{\partial y}\left(\frac{\rho^2 D}{\rho_w^2}\frac{\partial \phi}{\partial y}\right), \quad (5)$$

where ϕ is the coupled species and enthalpy function. If similarity methods are used, then the coupling function (ϕ) can be represented by a 3rd order polynomial:

$$\phi = a_0 + a_1\eta_\phi + a_2\eta_\phi^2 + a_3\eta_\phi^3, \quad (6)$$

$$\eta_\phi = y/\delta_\phi,$$

with coordinates η defined as the y-direction normalized by the thermal boundary layer thickness (δ_ϕ). The coefficients of the polynomial (a_i) are obtained by applying no-slip and no-penetration boundary conditions. The coefficients are [21]

$$\begin{aligned} a_0 &= 1, \\ a_1 &= 2/B\left[1 - (3B/2+1)^{(1/2)}\right], \\ a_2 &= -2a_1 - 3, \\ a_3 &= a_1 + 2\ . \end{aligned}$$

Using similarity variables with η, the energy equation can then be written as

$$I_\phi \delta_\phi \frac{d}{dx}\left[u\delta_\phi\right] = -(a_1)\rho^2 D[B+1], \quad (7)$$

$$I_\phi = \int_0^1 (1-f)\phi d\eta, \quad (8)$$

where δ_ϕ is the thermal boundary layer thickness, u is the freestream flow velocity, and f is the normalized velocity profile. On the right-hand side of Eq. (7), a_1 is the first coefficient in the coupling function polynomial, and ρ and D are the fuel density and mass diffusivity, respectively. The adiabatic mass transfer number is defined as

$$B = \frac{(Q_c/r)Y_{O_2,\infty} - c_p\left(T_{ig} - T_\infty\right)}{Q_g}\ . \quad (9)$$

The adiabatic B-number is a material property, with the first term in the numerator ($(Q_c/r)Y_{O2,\infty}$) representing the ratio of the energy released by combustion, where Q_c is the heat of combustion for the fuel, r is the stoichiometric oxygen-fuel mass ratio, and $Y_{O2,\infty}$, is the mass fraction of Oxygen, assumed to be 0.23 for air. The second term in the numerator ($c_p(T_{ig} - T_\infty)$) is the energy required to raise the gas from ambient (T_∞) to ignition temperature (T_{ig}), where c_p is the specific heat of air. The numerator is balanced by the heat of gasification (Q_g), which represents the energy required to gasify the solid fuel which was initially at ambient temperature. The adiabatic B-number assumes no losses, meaning

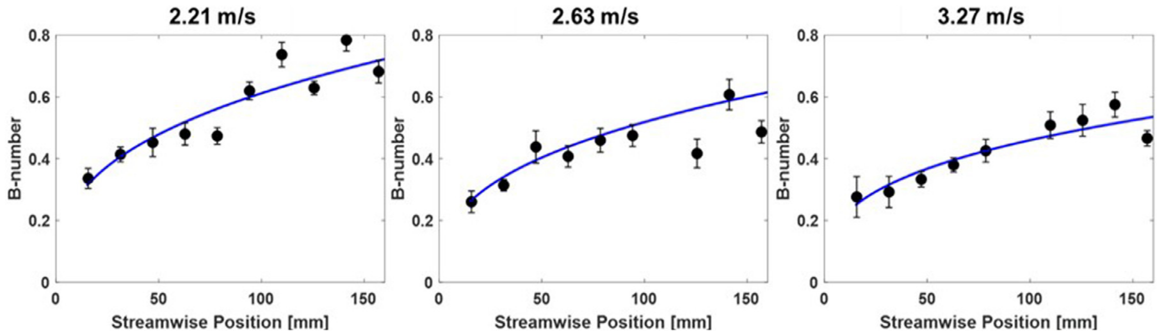

Fig. 6. Experimental *B*-numbers obtained for an array with a spacing of 1.25 cm and corresponding power-law regression line. At this spacing, the 2.21 m/s flow (left) is characterized as continuous flame spread while the 2.63 m/s (center) and 3.27 m/s (right) flows exhibit discrete flame behavior.

that the heat generated through combustion is used to heat the oxidizer and evaporate the fuel at the surface. The heat flux under zero mass transfer, i.e., the heat flux that would impinge on the next unignited fuel cylinder in the array, is estimated by Annamalai [21] and Spalding [23] as

$$\dot{q}'' = \left[\frac{B^2}{\ln(1+B)}\right]\frac{\rho DQ_g(-a_1)x^k}{(\delta_\phi/x)}. \tag{10}$$

The heat flux then depends on the adiabatic *B*-number, material properties (ρ and Q_g), the spatial distance (x), where k is a similarity exponent (–1/2), and the boundary layer thickness (δ_ϕ). The energy integral equation (Eq. (7)) is then rearranged and integrated to extract the boundary layer thickness (δ_ϕ):

$$\delta_\phi/x = \sqrt{\frac{(-a_1)(B+1)}{2I_\phi PrRe}}\ . \tag{11}$$

Solving Eq. (11) requires knowing the normalized velocity profile f due to the dependence on the coupling integral I_φ (Eq. (8)). Similar to the coupling function polynomial, the form of the velocity profile polynomial is given by Spalding [23] as

$$f = c_0 + c_1\eta_u + c_2\eta_u^2 + c_3\eta_u^3, \tag{12}$$

$$\eta_u = y/\delta_u\ .$$

The coefficients are outlined by Annamalai [21] and take a similar form to those for ϕ. Once I_φ is evaluated, the heat flux in the impinging plume can be determined using Eq. (10) [21,23].

4.2. B-number analysis

In this study, a *B*-number model will be developed to act as input for the stagnation-point heat flux (Eq. (10)). This model acts as a surrogate for the changes in the mass-transfer conditions due to different spacings and flow speeds. Although the theory in Section 4.1 relies on the adiabatic *B*-number, which is constant, it is replaced by the proposed empirical *B*-number model. To start, the experimental ignition times are used to calculate the heat flux based on Eq. (2). This experimental heat flux is then used as the heat flux in Eq. (10) to calculate the *B*-number. In this manner, the *B*-number is obtained for each dowel position for a given spacing/flow-velocity condition.

Fig. 6 presents the *B*-number results for an array with a spacing of 1.25 cm at three flow speeds. This process was repeated for each spacing/flow-velocity condition. A power-law regression was fit to each data set in the form of $B = Ax^p$. The power-law regression is used to develop the *B*-number model and to aid in the analysis of the *B*-number trends for different flow and spacing conditions. Because the *B*-number is calculated from the ignition time data, it represents the integrated *B*-number evolution of the dowel array system, which incorporates losses, up to ignition at that dowel position.

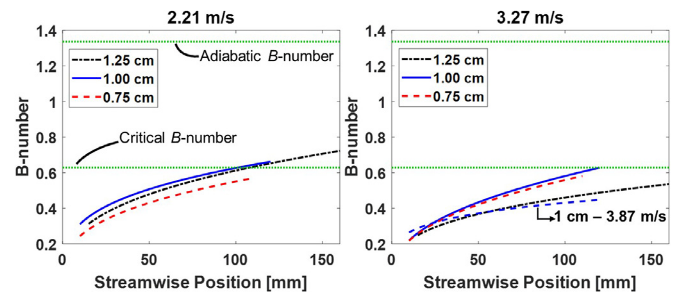

Fig. 7. *B*-number trends for 0.75-, 1.00-, and 1.25-cm spacing at low (left) and high (right) flow speeds. At a spacing of 1.25 cm, flame spread quenches at flow speeds higher than 3.27 m/s. At a spacing of 1 cm, the fastest flow speed at which flames could propagate was 3.87 m/s, which is plotted for reference.

As the flame spreads down the dowel array, the *B*-number continues to increase as more dowels burn simultaneously. The additional flaming dowels lead to higher cumulative heat flux, resulting in the acceleration of the flame spread and an increase in the *B*-number with respect to the dowel position.

As the flow conditions approach the quenching boundary, as seen with the 3.27 m/s flow in Fig. 6, the *B*-number curves flatten and approach a constant value across the dowel array. Under these high flow speeds, the flame is highly discretized, so that each dowel burns independently. Thus, the cumulative heat flux, which is associated with a growing flame within the continuous (i.e., low flow speed) regime, is reduced. Although the flame resists merging in the discrete regime, some influence from the burning upstream dowels is apparent.

The trends for other spacings follow similar behavior. Fig. 7 shows the *B*-number power-law regression as the flame propagates down arrays with a spacing of 0.75, 1.00, and 1.25 cm at low (2.21 m/s, left) and high (3.27 m/s, right) flow speeds. It is important to note that, at a speed of 2.21 m/s, a continuous flame spread regime is observed for all spacings, while only the 0.75-cm spacing exhibits continuous flame spread at a flow of 3.27 m/s. Plotted alongside the *B*-number curves in Fig. 7 is the adiabatic *B*-number for a wood fuel (1.34) calculated using Eq. (9) [8,9,21] and the critical *B*-number (0.63). The critical *B*-number can be expressed as

$$B_c = \frac{(Q_c/r)Y_{O_2,\infty} - c_p(T_{ig} - T_\infty)}{Q_g + L}, \tag{13}$$

where the variables are the same as in Eq. (9) but with the addition of a loss term (L). The loss term was taken to be approximately 2070 kJ/kg for wood as provided by Quintiere [28]. The critical *B*-number is a combination of material properties and the flow scenario, representing the point at which flames cannot prop-

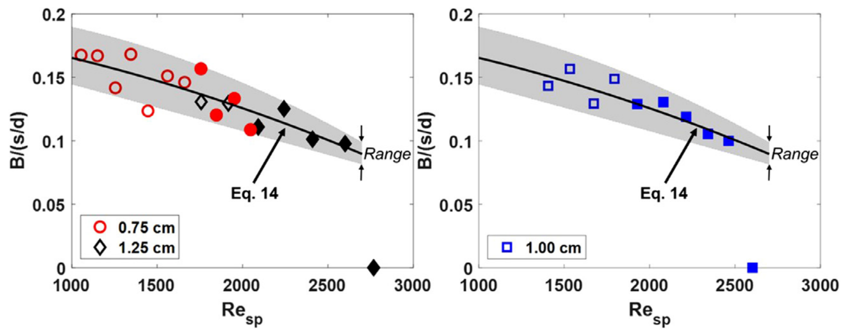

Fig. 8. Average dowel array scaled B-numbers plotted against the spacing-based Reynolds number. The plot on the left presents the data used for the regression and that on the right shows the regression predictions for a spacing of 1.00 cm. The filled markers represent discrete flame behavior. Also shown are the correlations of Eq. (14). (For interpretation of the references to color in this figure legend, the reader is referred to the web version of this article.)

agate along the surface due to losses [31]. The *B*-numbers observed here are much lower than those typically used in other studies and are able to sustain fire spread when they are as low as 40 to 50% of the free convection critical *B*-number. Generally, fire spread cannot be sustained at less than critical *B*-numbers. However, in the present study, the array configuration of the fuel combined with the forced flow allows for the flame spread to persist at low *B*-numbers. For a continuous fuel that is in the process of igniting, the preceding space where the flame exists contains fuel that is pyrolyzing or already ignited. With a discrete fuel configuration, however, that space preceding the fuel is empty. This spacing allows additional heat flux and oxygen to be delivered to the discrete element rather than absorbed by the preceding fuel in a continuous configuration; a similar phenomenon is observed in the vacancies of wooden crib fires [25,26]. Furthermore, because multiple array positions will be on fire simultaneously, the forced flow delivers additional heat from these upstream elements to the igniting element position, sustaining flame spread at what were previously understood as sub-critical *B*-numbers.

With larger spacings, because the flame must work harder to sustain fire spread under the same flow conditions due to the increased distance between fuel elements, the *B*-number generally increases compared to smaller spacings towards the end of the flame propagation. As observed in Fig. 6, the curves flatten as the flow speed increases. As the flow speed blow-off boundary is approached, the trend in the *B*-number reaches a similar asymptote for multiple spacings. This asymptote can be seen in Fig. 7 (right), where the 1.25-cm spacing is at the fastest flow speed that will sustain propagation, and the same condition is shown for 1.00-cm spacing at a speed of 3.87 m/s.

The power-law regressions for the *B*-number data obtained from the experimental ignition times (Fig. 6) were then evaluated to obtain the average *B*-number for dowel positions 5 to 10 for a fixed spacing/flow-speed condition. Because the *B*-numbers here are based on an average of the experimental ignition times as the flame ignites consecutive dowel positions, it is more analogous to an array or system *B*-number than to that of an individual dowel. Furthermore, by averaging the *B*-number, the average cumulative effect of the burning upstream dowels is embedded in the results.

Fig. 8 (left) displays the average dowel array system *B*-number for spacings of 0.75 and 1.25 cm plotted against the spacing-based Reynolds number (Re_{sp}).The spacing is used instead of the typical diameter as the length scale. The spacing was chosen for the length scale in *Re* because it represents the distance the flame must overcome in order to heat the next dowel. Likewise, the *B*-number is scaled by the spacing to diameter ratios ($s/d = 3.36$ and 4.94). Discrete flame behavior is denoted by the filled plot markers. By collapsing the data, the trends in Figs. 6 and 7 are explicitly apparent for changing flow speed and spacing conditions, including the gradual decrease in the *B*-number as flow speeds increase. Furthermore, as the array approaches blow-off conditions, the critical scaled *B*-number is in the range of 0.085–0.090.

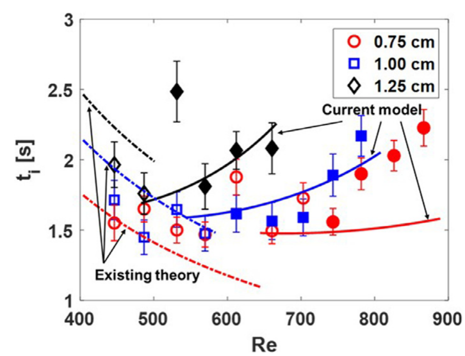

Fig. 9. Experimental and predicted time-to-ignition results for arrays with a spacing of 0.75, 1.00, and 1.25 cm for the full range of flow speeds tested. The filled-in markers represent discrete flame behavior. (For interpretation of the references to color in this figure legend, the reader is referred to the web version of this article.)

A quadratic regression based on the data from the spacings of 0.75 and 1.25 cm is shown to fit reasonably well ($R^2 = 0.72$):

$$\frac{B}{(s/d)} = -\left(1.5 \times 10^{-9}\right)Re_{sp}^2 - \left(3.898 \times 10^{-5}\right)Re_{sp} + 0.208 \ . \tag{14}$$

Using the empirical *B*-number regression as an approximate *B*-number model predicts the 1.00-cm spacing well (Fig. 8, right). This *B*-number model (Eq. (14)) serves as input for heat flux estimation (Eq. (12)) rather than the adiabatic *B*-number, thus accounting for changes in the fire spread caused by different spacing and flow conditions.

4.3. Results and discussion

Utilizing Eq. (14) as the *B*-number input to the heat flux estimation (Eq. (10)) and evaluating the thermally thick time to ignition (Eq. (2)), flame spread is modeled for a range of freestream Reynolds numbers (*Re*) covering the discrete flame behavior regimes. The model was not extended to the continuous flame behavior regime at lower *Re* due to the increased influence of buoyancy at slower flow speeds. Because the model is based on the stagnation point flow of a single cylinder, these conditions are reached at higher *Re* where the discrete flame behavior was observed.

The experimental results for the 0.75-, 1.00-, and 1.25-cm spacings are plotted in Fig. 9 alongside the *B*-number heat flux model. The experimental times shown are the average of the experimental times to ignition for dowels 5 to 10, with the filled markers representing the discrete flame behavior regimes. Additionally, predictions based on a *Nu-Re* model for cylinder banks in cross-flow [32] for the same conditions are displayed.

In the experimental data, the time to ignition decreases slightly as the flow speed initially increases. Just before the onset of discrete flame behavior, the time to ignition achieves a minimum. Once discrete flame spread begins (at approximately $Re = 700$ and $Re = 660$ for spacings of 0.75 and 1.00 cm, respectively), the flow no longer accelerates the flame spread as ignition times increase with increasing flow speeds until reaching the blow-off limit. The onset of discrete flame spread coincides with the fragmentation of the flame due to the cylinder wake flow structures interacting with the flame [18]. Increasing the spacing causes the flow structures to further influence the inter-cylinder region, resulting in discrete flame spread beginning at a lower *Re*. Furthermore, a larger spacing reduces the *Re* at which the flame ceases to propagate [19]. For instance, the 1.25-cm spacing ceases to propagate at around $Re = 700$, whereas, at a spacing of 0.75 cm, the flame propagates up to $Re = 900$. The stronger influence of turbulence and mixing due to faster flow speeds and larger spacings [19,20] leads to the induction time playing a larger role in the time to ignition, as determined by Niioka et al. [16].

Prior to the onset of discrete flame spread, the *Nu-Re* model accurately predicts the flame spread for spacings of 1.00 and 1.25 cm. However, once the flame behavior transitions to a discrete regime, the *Nu-Re* model deviates and calculates an increasingly faster flame spread as *Re* increases. Even though the *Nu-Re* relationship used here is based on a cylinder bank heat transfer [32], it cannot capture the decrease in heat flux associated with discrete flame spread.

In contrast, the proposed *B*-number model captures the ignition times increasing with higher *Re* and follows the slowing flame spread trend. Furthermore, the predictions for the 1.00-cm spacing are in good agreement with the experimental data. By incorporating the *B*-number model into the heat flux estimation, the effects of turbulence and increased mixing on the combustion efficiency are represented. Additionally, because the *B*-number estimation is based on the experimental time to ignition, the cumulative influence of the upstream burning dowels is implicitly embedded. In comparison, most *Nu-Re* models are developed based on non-reacting scenarios and, as demonstrated in Fig. 9, may not be suitable for all conditions.

It is apparent, however, that this method performs comparatively worse at a spacing of 0.75 cm. The increasing accuracy as the spacing increases could be attributed to the applicability of the heat flux model. As the gap between fuel elements increases, the fuel arrangement conditions approach that of a single cylinder. The flow structures that are formed behind tandem cylinders in cross-flow are dependent, in part, on the spacing-to-diameter ratio [33,34]. Below a certain spacing, the influence of these flow structures may be reduced due to greater flow blockage. At the smallest spacing (0.75 cm), the conditions may be such that the fire spread is better represented by a flat plate model than cylinders in cross-flow.

Conclusion

Existing *Nu-Re* heat transfer relationships for single cylinders and cylinder banks have been demonstrated to be accurate only up to a certain point for flame spread predictions for dowel arrays. After the onset of discrete flame behavior, the flame spread begins to slow down with increasing flow speeds. By contrast, the *Nu-Re* models predict an increasingly rapid flame spread. This discrepancy can be attributed to the combustion reaction and increased flow effects, such as vortex interactions, at a higher *Re* induced by the dowel cylinders. Heat flux estimation based on the single-cylinder stagnation-point flow that incorporates the *B*-number was adapted for dowel array predictions. The *B*-number represents a practical means for incorporating complex flow–flame interactions into heat flux predictions. Successful flame-spread modeling relies heavily on an accurate representation of the heat flux. It was shown that, by using the *B*-number approach, the deviations exhibited by the *Nu-Re* disappeared, and the flame spread was predicted reasonably accurately.

However, it seems that the applicability of the adapted stagnation flow model is limited to larger spacings. At a spacing of 0.75 cm, the gaps between cylinders may be at a width that prevents flow entrainment and mixing, rendering the conditions more similar to a flat plate than cylinders in cross-flow. Furthermore, under all spacing conditions, the current approximation neglects cumulative heating effects from upstream cylinders that may still be burning and contributing to the fire spread.

Declaration of Competing Interest

The authors declare that they have no known competing financial interests or personal relationships that could have appeared to influence the work reported in this paper.

Acknowledgment

This work was supported by U.S. DOD/EPA/DOE Strategic Environmental Research Development Program (SERDP, Project Number: RC-2641). Seong-kyun Im was supported by Korea University research grants.

References

[1] K. Hoover, L.A. Hanson, Wildfire statistics, Congressional research service, 2021. https://fas.org/sgp/crs/misc/IF10244.pdf.

[2] H.W. Emmons, Fire in the forest, Fire Res. Abstr. Rev. 5 (1963) 163–175.

[3] M.A. Finney, J.D. Cohen, S.S. McAllister, W.M. Jolly, On the need for a theory of wildland fire spread, Int. J. Wildland Fire. 22 (2013) 25–36, doi:10.1071/WF11117.

[4] R.C. Rothermel, A mathematical model for predicting fire spread in wildland fuels, USDA For. Serv. Res. Pap. INT USA (1972) 40 http://www.snap.uaf.edu/webshared/JenNorthway/AKFireModelingWorkshop/AKFireModelingWkshp/FSProAnalysis Guide References/Rothermel 1972 INT-115.pdf.

[5] W.L. Fons, Analysis of fire spread in light forest fuels, J. Agric. Res. 72 (1946) 93–121.

[6] J. Park, J. Brucker, R. Seballos, B. Kwon, Y.-T.T. Liao, Concurrent flame spread over discrete thin fuels, Combust. Flame. 191 (2018) 116–125, doi:10.1016/j.combustflame.2018.01.008.

[7] W. Cui, Y.-T.T. Liao, Experimental study of upward flame spread over discrete thin fuels, Fire Saf. J. 110 (2019) 102907, doi:10.1016/j.firesaf.2019.102907.

[8] M.J. Gollner, Y. Xie, M. Lee, Y. Nakamura, A.S. Rangwala, Burning behavior of vertical matchstick arrays, Combust. Sci. Technol. 184 (2012) 585–607, doi:10.1080/00102202.2011.652787.

[9] L. Jiang, Z. Zhao, W. Tang, C. Miller, J.H. Sun, M.J. Gollner, Flame spread and burning rates through vertical arrays of wooden dowels, Proc. Combust. Inst. 000 (2018) 1–8, doi:10.1016/j.proci.2018.09.008.

[10] M. Vogel, F.A. Williams, Flame propagation along matchstick arrays, Combust. Sci. Technol. 1 (1970) 429–436, doi:10.1080/00102206908952223.

[11] J.M. Prahl, J.S. Tien, Preliminary investigations of forced convection on flame propagation along paper and matchstick arrays, Combust. Sci. Technol. 7 (1973) 271–282, doi:10.1080/00102207308952367.

[12] T. Beer, Fire propagation in vertical stick arrays: the effects of wind, Int. J. Wildland Fire. 5 (1995) 43–49, doi:10.1071/WF9950043.

[13] M.F. Wolff, G.F. Carrier, F.E. Fendell, Wind-aided firespread across arrays of discrete fuel elements. I. Theory, Combust. Sci. Technol. 77 (1991) 261–289, doi:10.1080/00102209108951731.

[14] M.F. Wolff, G.F. Carrier, F.E. Fendell, Wind-aided firespread across arrays of discrete fuel elements. II. Experiment, Combust. Sci. Technol. 77 (1991) 261–289, doi:10.1080/00102209108951731.

[15] M.A. Finney, J.D. Cohen, J.M. Forthofer, S.S. McAllister, M.J. Gollner, D.J. Gorham, K. Saito, N.K. Akafuah, B.A. Adam, J.D. English, Role of buoyant flame dynamics in wildfire spread, Proc. Natl. Acad. Sci. 112 (2015) 9833–9838, doi:10.1073/pnas.1504498112.

[16] T. Niioka, M. Takahashi, M. Izumikawa, Gas-phase ignition of a solid fuel in a hot stagnation-point flow, Symp. Int. Combust. 18 (1981) 741–747, doi:10.1016/S0082-0784(81)80078-1.

[17] T. Niioka, Ignition time in the stretched-flow field, Symp. Int. Combust. 18 (1981) 1807–1813, doi:10.1016/S0082-0784(81)80186-5.
[18] G. Di Cristina, S. Kozhumal, A. Simeoni, N. Skowronski, A. Rangwala, S. Im, Forced convection fire spread along wooden dowel array, Fire Saf. J. 120 (2021) 103090, doi:10.1016/j.firesaf.2020.103090.
[19] G. Di Cristina, N.S. Skowronski, A. Simeoni, A.S. Rangwala, S. Im, Flame spread behavior characterization of discrete fuel array under a forced flow, Proc. Combust. Inst. 38 (2021) 5109–5117, doi:10.1016/j.proci.2020.05.035.
[20] N. Hosseini, M.D. Griffith, J.S. Leontini, The flow past large numbers of cylinders in tandem, J. Fluids Struct. 98 (2020) 103103, doi:10.1016/j.jfluidstructs.2020.103103.
[21] K. Annamalai, M. Sibulkin, Flame spread over combustible surfaces for laminar flow systems part I: excess fuel and heat flux, Combust. Sci. Technol. 19 (1979) 167–183, doi:10.1080/00102207908946878.
[22] K. Annamalai, M. Sibulkin, Flame spread over combustible surfaces for laminar flow systems part II: flame heights and fire spread rates, Combust. Sci. Technol. 19 (1979) 185–193, doi:10.1080/00102207908946879.
[23] D.B. Spalding, Mass transfer in laminar flow, Proc. R. Soc. Lond. Ser. Math. Phys. Sci. 221 (1954) 78–99, doi:10.1098/rspa.1954.0006.
[24] T. Niioka, F.A. Williams, Ignition of a reactive solid in a hot stagnation-point flow, Combust. Flame. 29 (1977) 43–54, doi:10.1016/0010-2180(77)90092-X.
[25] V. Gupta, A.F. Osorio, J.L. Torero, J.P. Hidalgo, Mechanisms of flame spread and burnout in large enclosure fires, Proc. Combust. Inst. (2020) S1540748920305241, doi:10.1016/j.proci.2020.07.074.
[26] V. Gupta, J.L. Torero, J.P. Hidalgo, Burning dynamics and in-depth flame spread of wood cribs in large compartment fires, Combust. Flame. 228 (2021) 42–56, doi:10.1016/j.combustflame.2021.01.031.
[27] A.C. Fernandez-Pello, The solid phase, Combustion Fundamentals Fire, Academic Press, New York (1995), pp. 31–100.
[28] J.G. Quintiere, Fundamentals of Fire Phenomena, John Wiley & Sons Ltd, 2006, doi:10.1002/0470091150.
[29] F. Incropera, D. DeWitt, T. Bergman, A. Lavine, Fundamentals of Heat and Mass Transfer, 7th ed., John Wiley & Sons, New York, 2011.
[30] F.A. Williams, Combustion theory: the Fundamental Theory of Chemically Reacting Flow Systems, 2nd ed, Benjamin/Cummings Pub. Co, Menlo Park, Calif, 1985.
[31] J.L. Torero, T. Vietoris, G. Legros, P. Joulain, Estimation of a total mass transfer number from the standoff distance of a spreading flame, Combust. Sci. Technol. 174 (2002) 187–203, doi:10.1080/713712953.
[32] W.A. Khan, J.R. Culham, M.M. Yovanovich, Convection heat transfer from tube banks in crossflow: analytical approach, Int. J. Heat Mass Transf. 49 (2006) 4831–4838, doi:10.1016/j.ijheatmasstransfer.2006.05.042.
[33] B.S. Carmo, J.R. Meneghini, S.J. Sherwin, Possible states in the flow around two circular cylinders in tandem with separations in the vicinity of the drag inversion spacing, Phys. Fluids. 22 (2010) 1–7, doi:10.1063/1.3420111.
[34] B.S. Carmo, J.R. Meneghini, S.J. Sherwin, Secondary instabilities in the flow around two circular cylinders in tandem, J. Fluid Mech. 644 (2010) 395, doi:10.1017/S0022112009992473.